Journal of Materials, Processing and Design (2026)
Clausius Scientific Press, Canada

DOI: 10.23977/jmpd.2026.100109
ISSN 2516-0923 Vol. 10 Num. 1

Material Removal Function Modelling Based on the Power Cosine Function (PCF) for Magnetorheological Finishing of Cylinder

Jiajia Ma[1,a], Wei Fan[1,b,*], Yunfei Zhang[1,c,*], Kuo Hai[1,d,*], Kailong Li[1,e]

[1]Institute of Machinery Manufacturing Technology, China Academy of Engineering Physics, Mianshan Road No. 64, Mianyang, China
[a]2835732297@qq.com, [b]weifan1127@hust.edu.cn, [c]zhangyf306@yeah.net, [d]haikuo_6s@126.com, [e]KaiLL_CAEP6@126.com
**Corresponding author*

Keywords: Magnetorheological finishing, material removal function, power cosine function

Abstract: In the magnetorheological finishing (MRF) process of cylindrical optical elements, the material removal function (RF) undergoes significant distortion due to curvature effects. The existing physical modelling methods require complex physicochemical measurements and struggle to decouple the influencing factors. The existing geometric modelling methods also has limitations such as insufficient parameters or ignoring the nonlinear distortion of curvature. In response to these challenges, this work proposes a pure geometric RF modelling method based on the power cosine function (PCF). By introducing 10 morphological coefficients, the method constructs a morphological flexible surface, which can accurately describe the RF profile under different curvatures and immersion depths, and supports rapid prediction of the RF under variable working condition. Compared with Schinhaerl's model, the experimental results show that the PCF method reduces the average peak removal rate error (APRRE), the average volumetric removal rate error (AVRRE), and the average contour error (ACE) by 42.9%, 63.5%, and 58.4%, respectively. The proposed method provides an effective modelling tool for high-precision and high-deterministic polishing of cylindrical optical elements.

1. Introduction

The increasing demand for high-precision cylindrical optical components in high-tech military and civilian fields[1], such as medical devices and satellite navigation, has driven the development of advanced manufacturing methods[2]. MRF has become a key technique for achieving high-precision and high-efficiency manufacturing of such components, owing to the stable removal function, minimal subsurface damage, and high material removal efficiency[3][4]. However, in the process of MRF, accurate prediction of the RF is a key factor affecting the convergence efficiency of component processing[5], especially in the processing of cylindrical components, where curvature effects cause significant distortion. Therefore, establishing a predictive model for the RF applicable to actual working condition is of great significance for achieving high-precision and high-efficiency

manufacturing of cylindrical components[6].

The existing RF modelling methods mainly include experimental methods, physical modelling methods and geometric modelling methods. Experimental methods derive the RF by collecting actual removal data from workpiece through experiments. However, the methods are costly and cannot directly provide the RF for complex surfaces with variant curvatures. Physical modelling methods establish dynamic equations in the polishing zone based on the Bingham fluid constitutive equation and lubrication theory, and solve the partial differential equations to obtain physical fields, and then adjust the influence coefficients according to the Preston hypothesis[7]. However, the existing physical modelling methods have several limitations. For distance, the modelling and prediction processes require physicochemical measurements, which reduces the efficiency of the derivation. Additionally, physicochemical and geometric factors cannot be effectively decoupled, which diminishes the stability of RF derivation. Furthermore, those methods are applicable only to planar, spherical, or aspherical surfaces, and unsuitable for cylindrical surfaces[8-13]. Geometric modelling methods involve constructing the RF using geometric models and reconstructing the RF profile based on experimental data. Schinhaerl et al.[14][15] proposed a model based on trigonometric functions, but the model contains only three adjustable parameters and insufficient for cylindrical surfaces with significant differences in principal curvatures. Han et al.[16] used a Gaussian mixture model, but the approach does not consider distortion caused by curvature effects, and the number of peaks in the RF is unstable. Yang et al.[17] proposed a linear correction method for conical surfaces. However, the linear approximation neglects the nonlinear distortion caused by curvature changes and fails to analyze the impact of immersion depth. Therefore, existing geometric modelling methods cannot accurately predict the RF of cylindrical MRF[18]-[20].

To address the aforementioned issues, this paper proposes a pure geometric modelling approach based on the power cosine function (PCF). By introducing morphological coefficients, the model can flexibly adapt to various surface shapes and accurately fit the RF using a small number of parameters. Additionally, when the process parameters change, the RF profile under new working condition can be rapidly generated without the need for complex physicochemical measurements. The main contributions of this paper include the establishment of a new PCF geometric model suitable for MRF removal function modelling of cylinder, achieving high accuracy with fewer parameters. The prediction ability of the method under variable working condition is verified by experiments

The remainder of this paper is arranged as follows. Section 2 introduces the PCF-based RF modelling method. Section 3 provides experimental validation, and Section 4 presents the conclusion.

2. PCF-based RF model

In this section, a pure geometric RF model for MRF of cylinder is established based on the PCF, including function morphology analysis, skeleton parameter extraction, construction of the complete analytical expression, and parameter identification method. Then, we describe how to predict the RF under variable working conditions by utilizing the relationship among the calibrated morphological coefficients, curvatures and immersion depths, along with the reference RF collected on the plane.

2.1. Definition of the PCF

As shown in Figure 1, the PCF is a composite function formed by two exponentiation parameters and a cosine function. The morphology of the function changes flexibly depending on the values of the exponentiation parameters, and it can be used to describe a variety of target shapes. The specific

form is given by

$$f(x;x_1,x_2,H,n_1,n_2)=H\cos^{2n_2}\left(\frac{\pi}{2}\left|\frac{x-x_2}{\Delta}\right|^{n_1}\right) \tag{1}$$

where $\Delta=x_2-x_1$. When $n_2=1$ and $n_1>1$, the function at the peak becomes smother as n_1 increases. When $n_2=1$ and $0<n_1<1$, the function at the peak becomes sharper as n_1 decreases. When $n_1=1$ and $n_2>1$, the function at the valley becomes smoother as n_2 increases. When $n_1=1$ and $0<n_2<1$, the function at the valley becomes shaper as n_2 decreases.

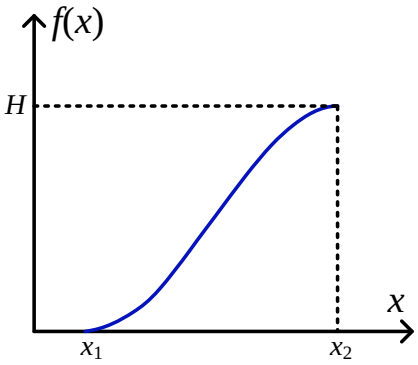

Figure 1: Power cosine function (PCF).

2.2. Extraction of skeleton parameters of the RF

As shown in Figure 2, the MRF RF exhibits a typical inverse "D" shape, and the profile can be approximated as the union of two semi-ellipses[11]. The specific expression is

$$\begin{cases}\left(\dfrac{x}{(1-k_h)L}\right)^2+\left(\dfrac{2y}{W}\right)^2=1 & x\le 0\\ \left(\dfrac{x}{k_hL}\right)^2+\left(\dfrac{2y}{W}\right)^2=1 & x>0\end{cases} \tag{2}$$

where L and W represent the total length and width of the RF, and k_h represents the head ratio.

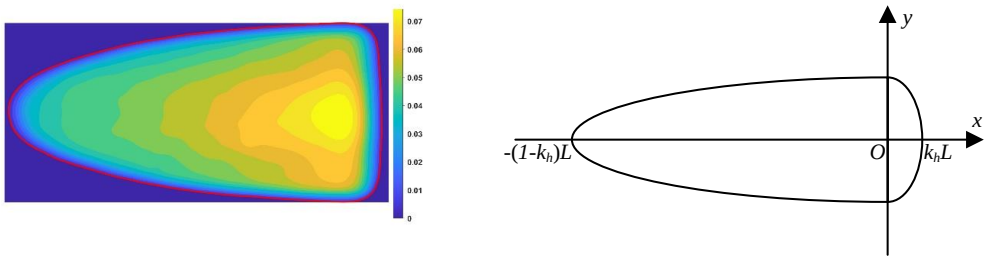

(a) (b)

Figure 2: The contour of RF: (a) Actual RF distribution; (b) Elliptical contour approximation.

The model provides an idealized geometric description of the RF skeleton. To determine the corresponding skeleton parameters (L,W,k_h) of the RF, the actual profile boundary of the RF must

be accurately identified. In this work, the canny operator[21][22] is adopted due to its high signal-to-noise ratio, precise localization, and robust detection of continuous edges, making it suitable for extracting the RF contour, which has a distinct main profile yet may exhibit minor local fluctuations.

The extraction procedure includes Gaussian filtering for noise reduction, gradient computation with non-maximum suppression for edge refinement, and dual-threshold detection for edge connection. And then the resulting contour points are treated as boundary samples and fitted using the least-squares method. The optimized skeleton parameters (L, W, k_h) define the effective region of the RF and provide constraints for subsequent modelling.

2.3. Construction of the PCF-based RF model

Based on the skeleton parameters obtained in Section 2.1 and 2.2, an analytical model of the RF is further established. The MRF RF exhibits pronounced asymmetry along the long-axis and symmetry along the short-axis. Accordingly, a normalized piecewise PCF is used to describe the profile along the long-axis, while a normalized PCF is adopted for the short-axis. The RF model is then constructed via a tensor product.

$$R(x,y) = R_{max} \cdot f_X(x) \cdot f_Y(x,y) \tag{3}$$

$$f_X(x) = \begin{cases} f\left(\frac{x}{L}; -(1-k_h), 0, 1, p_1, p_2\right) & x \in [-(1-k_h)L, 0] \\ f\left(\frac{x}{L}; k_h, 0, 1, p_3, p_4\right) & x \in (0, k_h L] \end{cases} \tag{4}$$

$$f_Y(x,y) = f\left(\frac{2y}{w(x)}; -1, 0, 1, p_5, p_6\right) \quad y \in [-\frac{w(x)}{2}, \frac{w(x)}{2}] \tag{5}$$

where $w(x)$ denotes the local width of the RF at position x.

For a given RF $\xi(x,y)$ under known curvature and immersion depth, the elliptical contour is first extracted using an edge detection algorithm, and the skeleton parameters L, W, k_h are obtained via the method described in Section 2.2. The morphological coefficients are then identified by solving the following least-squares problem, which yields the analytical expression of the RF.

$$\min_{R_{max}, p_1, \ldots, p_6} \sum_i (\xi(x_i, y_i) - R(x_i, y_i))^2 \tag{6}$$

2.4. Prediction of RF under varying working condition

The morphological parameters of the RF include the length L, width W, head ratio k_h, the peak removal rate R_{max}, and dimensionless shape coefficients $p_1, \ldots, p_6$. Among these, the dimensionless parameters $k_h, p_1, \ldots, p_6$ depend only on the curvature and immersion depth, and are independent of physicochemical factors such as polishing fluid viscosity and the polishing wheel rotational speed. Under the modelling condition, for a given curvature and immersion depth, these coefficients are identified from experimental data. By contrast, L and W are assumed to be linearly proportional to the corresponding dimensions of a reference planar RF under actual working condition. Therefore, based on the interpolated dimensionless coefficients obtained with the same curvature and immersion depth under the modelling working condition and the measured planar RF under the actual working condition, the RF with any desired immersion depth and curvature under the actual working condition can be efficiently predicted.

3. Simulation and experiment

The experiments for validating the RF model proposed are conducted on a self-developed five-

axis MRF machine. The ribbon flow direction is set perpendicular to the cylindrical generatrix direction. Spot data are collected under the modelling condition for convex cylindrical surfaces with the curvature radii of -400mm, -615mm, as well as a planar surface. The immersion depths are set to 0.2mm, 0.3mm, 0.4mm, and the spot-taking time is fixed as 3s. The RFs are fitted using the method described in Section 2.3. The fitting performance is evaluated by analyzing the peak removal rate error (PRRE), the volumetric removal rate error (VRRE) and the contour error (CE) between the fitted and actual RFs. The fitting results are compared with those obtained using Schinhaerl's model, as shown in Figure 3.

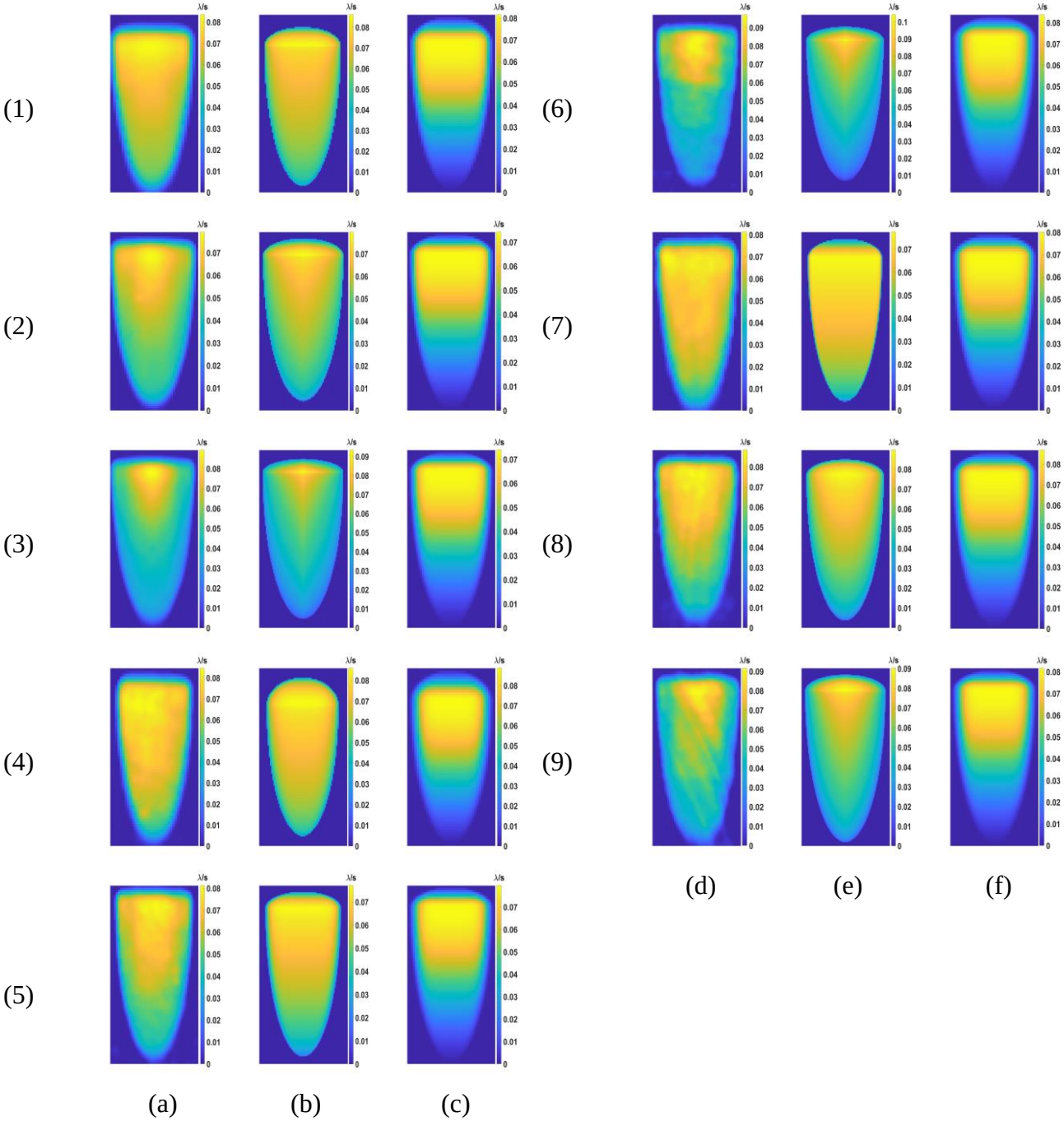

Figure 3: The fitting results of different methods: (a), (d) Actual RF; (b), (e) Proposed method; (c), (f) Schinhaerl's model.

The PRRE, VRRE, and CE of the fitted RFs obtained by the proposed method and Schinhaerl's model are presented in Figure 4. The comparison shows that the APRRE of the proposed method is 0.0266, while that of Schinhaerl's model is 0.0674, indicating a reduction of 60.5%. The proposed method achieves the AVRRE of 0.0352, compared with 0.1510 for Schinhaerl's model, corresponding to a reduction of 76.7%. Moreover, the ACE is reduced from 0.2192 to 0.0692, representing a 68.4% reduction. Overall, the proposed method significantly outperforms Schinhaerl's model in all error metrics.

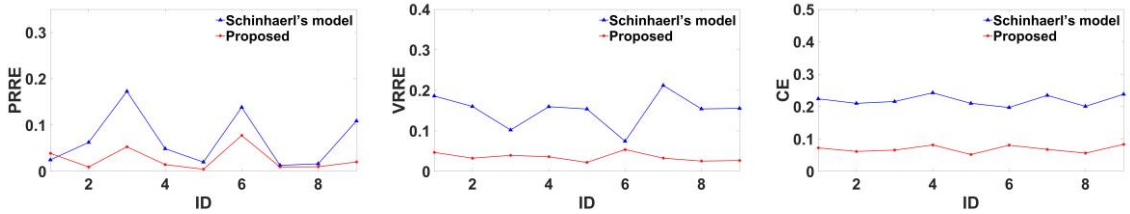

(a) (b) (c)

Figure 4: The RF fitting results of different methods: (a) PRRE; (b) VRRE; (c) CE.

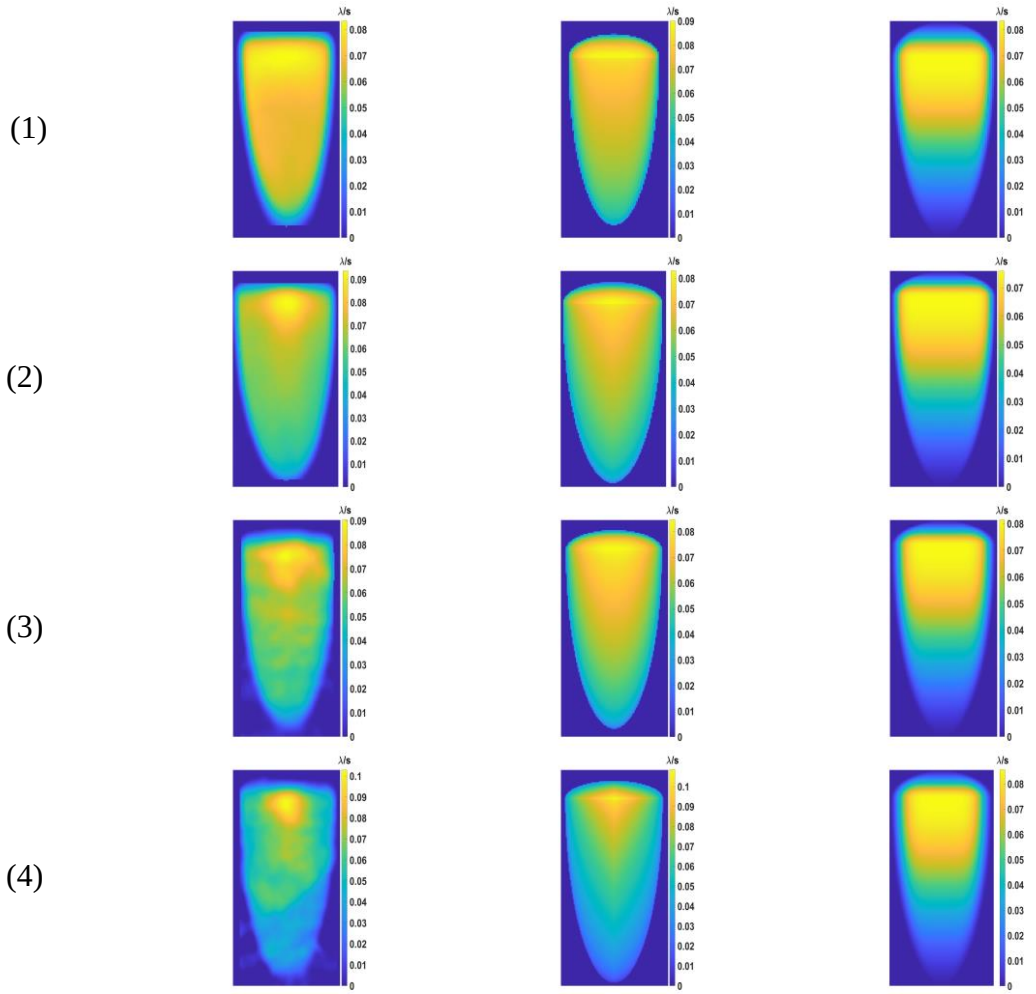

(1)

(2)

(3)

(4)

(a) (b) (c)

Figure 5: The prediction results of different methods: (a) Actual RF; (b) Proposed; (c) Schinhaerl's.

Under the actual working condition, polishing spots are collected on both a plane and a cylindrical surface with curvature radii of -608mm. The immersion depths are set to 0.2mm, 0.3mm

and 0.4mm with a fixed spot-taking time of 3s. The planar spot at an immersion depth of 0.4mm is used as the reference spot. The proposed method and Schinhaerl's model are compared in terms of PRRE, VRRE, and CE between the predicted and actual RFs. Due to the insufficient quality of the cylindrical spot collected at an immersion depth of 0.2mm, only cylindrical RFs at immersion depths of 0.3mm and 0.4mm are compared. The comparison results are shown in Figure 5 and Figure 6.

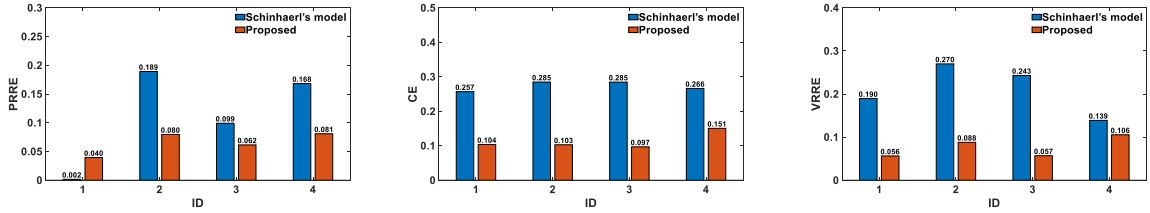

(a) (b) (c)

Figure 6: The RF prediction results of different methods: (a) PRRE; (b) VRRE; (c) CE.

The results show that the proposed method achieves an APRRE of 0.0654, an AVRRE of 0.0768, and an ACE of 0.1135. In comparison, Schinhaerl's model yields an APRRE of 0.1146, an AVRRE of 0.2104, and an ACE of 0.2732. Overall, the proposed method outperforms Schinhaerl's model across all the error metrics, demonstrating its capability for efficient prediction of the RF under actual working condition.

4. Conclusions

This work addresses the morphological distortion of the RF induced by curvature effects for MRF of cylindrical optical elements. A pure geometric modelling method based on the PCF is proposed. By introducing ten morphological coefficients, the proposed method can flexibly describe the RF under different working condition and enables efficient prediction of RF morphology under varying curvatures and immersion depths. Experiment results demonstrate that compared with Schinhaerl's model, the proposed method reduces the APRRE, AVRRE, and ACE by 42.9%, 63.5%, and 58.4%, respectively. Overall, the proposed method provides a new pathway for high-precision and high-efficiency MRF of cylindrical optical components.

Acknowledgements

This research is supported by National Natural Science Foundation of China (61605182, 12162008, 52505535), and National Program of China (J0162-2527-QT). The authors gratefully acknowledge Jun Liu, a technician from Institute of Machinery Manufacturing Technology of China Academy Engineering Physics, providing the assistance for the experimental validation.

References

[1] Chen, B., Wu, Q., Tang, Y., Fan, J., Chen, X., Sun, Y. (2023) Design of an optical system for generating annular-focused beams using a conical mirror and a parabolic cylindrical mirror. Optik (Stuttgart), 281, 170625.
[2] Li, J., Zhou, L., Ma, H., Zhang, Q. (2023) Ultra-precision grinding of monocrystalline silicon cylindrical mirror. Journal of Physics. Conference Series, 2591(1), 12005.
[3] Wang, W., Ji, S., Zhao, J. (2024) Review of magnetorheological finishing on components with complex surfaces. International Journal of Advanced Manufacturing Technology, 131(5-6), 3165–3191.
[4] Gao, Q., Wang, S., Shi, F., Zhang, N., Hao, Q., Su, P., Liu, F. (2026) Dwell time calculation and curvature effect compensation method of magnetorheological finishing for large-aperture aspheric optics. Proceedings of SPIE, the International Society for Optical Engineering, 14000, 140004S-140004S-8.
[5] Zhong, X., Fan, B., Wu, F. (2017) High-accuracy process based on the corrective calibration of removal function in

the magnetorheological finishing. Optical Engineering, 56(8), 084109.
[6] Yan, K., Li, L., Cheng, R., Liu, X., Li, X., Bai, Y., Zhang, X. (2024) Mapping model of ribbon contour and tool influence function based on distributed parallel neural networks in magneto-rheological finishing. Optics Express, 32(16), 27099.
[7] DeGroote, J. E., Marino, A. E., Wilson, J. P., Bishop, A. L., Lambropoulos, J. C., Jacobs, S. D. (2007) Removal rate model for magnetorheological finishing of glass. Applied Optics, 46(32), 7927–7941.
[8] Zhang, L., Li, W., Lu, M., Lin, J., Liu, Y., Liu, C. (2023) Material removal mechanism of fused silica glass in magnetorheological finishing. International Journal of Advanced Manufacturing Technology, 128(3-4), 1271-1289.
[9] Chen, S., Weng, Y., Yao, B. (2024) Material removal model for magnetorheological polishing considering shear thinning and experimental verification. Materials Today Communications, 38, 108475.
[10] Lu, M., Yang, Y., Liu, Y., Zhang, L. (2025) Modelling and process analysis of material removal rate in magnetorheological polishing of fused quartz glass. Journal of the Brazilian Society of Mechanical Sciences and Engineering, 47(10), 471.
[11] Liu, J., Li, X., Zhang, Y., Tian, D., Ye, M., Wang, C. (2020) Predicting the Material Removal Rate (MRR) in surface Magnetorheological Finishing (MRF) based on the synergistic effect of pressure and shear stress. Applied Surface Science, 504, 144492.
[12] Luo, B., Zhang, L., Yan, Q., Jiao, Z., Fu, Y., Luo, J. (2025) Material removal model for magnetorheological dynamic pressure polishing based on gap-varying and experimental verification. International Journal of Advanced Manufacturing Technology, 138(7), 3497–3515.
[13] Cheng, R., Li, L., Xue, D., Li, X., Bai, Y., Luo, X., Zhang, X. (2023) Accurately predicting the tool influence function to achieve high-precision magnetorheological finishing using robots. Optics Express, 31(21), 34917.
[14] Schinhaerl, M., Smith, G., Stamp, R., Rascher, R., Smith, L., Pitschke, E., Sperber, P., Geiss, A. (2008) Mathematical modelling of influence functions in computer-controlled polishing: Part I. Applied Mathematical Modelling, 32(12), 2888-2906.
[15] Schinhaerl, M., Smith, G., Stamp, R., Rascher, R., Smith, L., Pitschke, E., Sperber, P., Geiss, A. (2008) Mathematical modelling of influence functions in computer-controlled polishing: Part II. Applied Mathematical Modelling, 32(12), 2907-2924.
[16] Han, Y., Zhu, W., Zhang, L., Beaucamp, A. (2020) Region adaptive scheduling for time-dependent processes with optimal use of machine dynamics. International Journal of Machine Tools & Manufacture, 156, 103589.
[17] Yang, J., Fan, W., Hai, K., Huang, W. (2023) The distortion law analysis and deduction of TIF for magnetorheological finishing of conical mirror, Opt. Precis. Eng. 31 (16) 2383–2394 (in Chinese).
[18] Song, C.: Study on the key techniques of magnetorheological finishing for off-axis aspheric optical elements (2012), Ph.D. Thesis, National University of Defense Technology (in Chinese).
[19] Zhang, J., Wang, H. (2021) Generic model of time-variant tool influence function and dwell-time algorithm for deterministic polishing. International Journal of Mechanical Sciences, 211, 106795.
[20] Yang, H., Zhang, Q., Zhu, Z., Fan, W., Zhang, Y., Huang, W. (2019) Dynamic approximation method for removal function size in magnetorheological finishing. Optical Engineering, 58(9), 095103.
[21] Canny, J. (1986) A Computational Approach to Edge Detection. IEEE Transactions on Pattern Analysis and Machine Intelligence, PAMI-8(6), 679-698.
[22] Song, R., Zhang, Z., Liu, H. (2017) Edge connection based Canny edge detection algorithm. Pattern Recognition and Image Analysis, 27(4), 740-747.